Photodissociation Dynamics of HN_3 and DN_3 at 157 nm

Kaijun Yuan, Yuan Cheng, Fengyan Wang, and Xueming Yang*

State key Laboratory of Molecular Reaction Dynamics, Dalian Institute of Chemical Physics, Chinese Academy of Sciences, 457 Zhongshan Road, Dalian 116023, China

Received: January 4, 2008; Revised Manuscript Received: April 3, 2008

Photodissociation dynamics of HN_3 at 157.6 nm have been studied using the H-atom Rydberg tagging time-of-flight technique. Product translational energy distributions and angular distributions have been measured. From these distributions, three H-atom channels are observed. The vibrational structure in the fast-H channel could be assigned to a progression in the N_3 symmetric stretching mode ($\nu_1 00$), together with a progression of the symmetric stretching mode with one quantum of bending motion ($\nu_1 10$). The broad translational energy distribution of the slow-H channel is energetically consistent with the cyclic-N_3 formation process or a triple product dissociation channel. Photodissociation of DN_3 was also investigated using the same technique. Isotope effect on the product translational energy distribution has been observed, in which the slow H-atom is clearly more pronounced.

Introduction

Photodissociation of hydrazoic acid (HN_3) has attracted much attention over the last two decades.[1] The hydrazoic acid molecule has been sought as the material capable of storing large amounts of energy in minimal mass or volume, a possible "high-energy-density-material", due to the fact that it is so unstable.[2] Because of its accessibility by various experimental techniques and high-level quantum chemical methods, this system has also been referred as a benchmark system for the study of polyatomic photochemical dynamics.

The UV absorption spectrum of HN_3 (Figure 1) is composed of at least four absorption systems between 150 and 300 nm: a weak one peaking at about 264.3 nm, two strong ones peaking around 204 and 190 nm, and an even stronger system around 157 nm, respectively.[3,4] These absorption features appear broad and nearly structureless. The weak feature at $\lambda > 220$ nm has been assigned in terms of excitation from the $\tilde{X}^1A'$ ground state to the $\tilde{A}^1A''$ first excited singlet electronic state. At shorter wavelengths, the $\tilde{B}^1A'$ and $\tilde{C}^1A''$ electronic states are optically accessible, and the resulting UV absorption spectrum is strong, but no discrete structure is present. The Rydberg state transition $\tilde{D}^1A' \leftarrow \tilde{X}^1A''$ is prominent at $\lambda < 170$ nm.

It was known that the spin and thermodynamically allowed dissociation channels at $\lambda > 200$ nm are

$$HN_3(\tilde{X}1A') \rightarrow H(2S) + N_3(\tilde{X}^2\Pi_g) \quad (1)$$

$$\rightarrow NH(a^1\Delta) + N_2(\tilde{X}^1\Sigma_g^+) \quad (2)$$

The detailed dynamics of channel 2 have been extensively studied at several different wavelengths.[5–9] Measurements of the NH ($a^1\Delta$) fragment vibrational state population distribution resulting from HN_3 photolysis in the range 220−290 nm reveal energetic onsets for products with $v = 1$ and $v = 2$. The observed population ratio $N_{v=1}/N_{v=0}$ is at maximum at $\lambda = 240$ nm.[9] Chu et al. [5] investigated the internal energy distributions in both the $N_2(\tilde{X}^1\Sigma_g^+)$ and NH ($a^1\Delta$) fragments from the 283 nm photolysis. They found that the N_2 fragment was produced mainly in its vibrational ground state with high rotational excitation, whereas the rotational excitation of the NH ($a^1\Delta$) fragment was quite small.

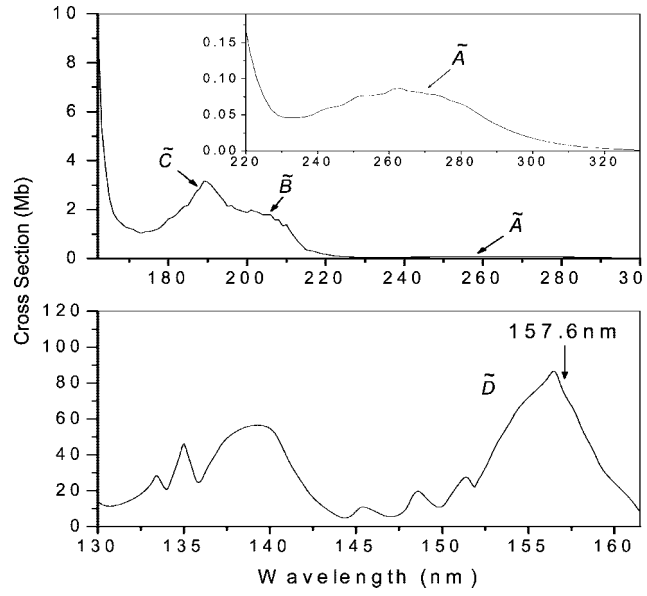

Figure 1. Absorption spectrum of HN_3 at room temperature (adapted from refs 3 and 4). The position of the photolysis excitation wavelength in this work is indicated by arrows (1 Mb = 1×10^{-18} cm^2).

Photodissociation dynamics of channel 1 have been investigated by Comes and co-workers by using H-atom laser-induced fluorescence (LIF) at 266, 248, 222, 193 and 122 nm.[10,11] Comparisons of the H atom LIF intensities with those resulting from H_2S photolysis led to estimates of the respective quantum yields for forming H atom products: $\Phi_{266} = 0.04$, $\Phi_{248} = 0.20$, $\Phi_{193} = 0.14$. Using H-ion TOF spectroscopy,[12] the H−N bond energy was determined to be $D_0(H-N_3) = 30850 \pm 400$ cm^{-1}. Because of the limited energy resolution of this technique, the resulting H-ion TOF profile was broad and poorly resolved. The result suggested that the N_3 internal energy distribution is very broad with its width of ~6000 cm^{-1}. The dominant features in this profile were assigned to a progression in the ν_1 symmetric

* To whom all correspondence should be addressed. E-mail: xmyang@dicp.ac.cn.

10.1021/jp800062t CCC: $40.75
Published on Web 05/24/2008

stretching mode of N_3 and the relative population of the (000):(100):(200):(300):(400) product states was found to be 0.09:0.19:0.28:0.29:0.15.

Recently, the high-*n* Rydberg H-atom time-of-flight (HRTOF) technique has also been employed to investigate the H-atom channel.[13–17] Cook et al.[13,14] reported the translational energy spectra of the $H + N_3(\tilde{X})$ products for photolysis wavelengths between 240 and 280 nm. On the basis of their experimental results and ab initio potential energy surface calculations, they concluded that the N_3 fragments were formed in the progression involving both the symmetric stretch mode ($\nu_1 00$) only and the symmetric stretch mode combined with one and two quanta of bending motion, ν_2. They used an impulsive model to reproduce the deduced $N_3(\tilde{X})$ product rotational energy disposal, obtained an impact parameter, $b = 1.26 \pm 0.05$ Å, and a refined measure of the H−N_3 bond strength, $D_0(H-N_3) = 30970 \pm 50$ cm^{-1}. Zhang et al.[15] have also used HRTOF to investigate the HN_3 photodissociation at 248 and 193 nm. They found that photolysis at 193 nm clearly leads to more internally excited N_3 radicals than does photolysis at all other wavelengths that have been studied. The observed product anisotropy parameter is clearly energy-dependent, implying multiple dissociation pathways are involved. More recently, Zhang et al.[16,17] reinvestigated the photodissociation of HN_3/DN_3 using the HRTOF method, spanning the range of photolysis wavelengths between 188 and 280 nm in roughly 5 nm steps. They have observed subtle yet striking changes in the photodissociation dynamics as the photolysis energy passes through ~5.6 eV. Their results suggest that a cyclic-N_3 formation channel is present, in addition to the linear-N_3 fragment channel.

The photolysis of HN_3 in the UV region has been studied in many experiments as shown above; however, little work has been done on the dynamics of the HN_3 photodissociation after excitation in the vacuum ultraviolet (VUV) region. In this work, we investigated the photodissociation dynamics of HN_3/DN_3 molecules using HRTOF technique at 157.6 nm. Product translational energy distribution and angular distribution have been measured by using polarized photolysis laser radiation in this study. Photodissociation mechanisms and the excited electronic states involved are discussed.

2. Experimental Section

The high-*n* Rydberg H-atom time-of-flight (HRTOF) technique utilized in this study has been described in detail elsewhere and only a brief description is presented here.[18,19] A skimmed pulsed molecular beam of HN_3, seeded in helium (mixing ratio ~2.5%, total pressure ~760 Torr), is crossed perpendicularly with the output of the 157.6 nm photolysis laser (VUV power 2−4 mJ, with the beam diameter ~10 mm), which was produced by a Lambda Physik LPX210I F_2 laser. The 157.6 nm radiation was polarized by a special 157.6 nm polarizer and focused by an MgF_2 lens. The H/D products from photodissociation were then excited to a high-*n* Rydberg level using a two-step excitation scheme: coherent VUV excitation at the Lyman-α wavelength (121.6 nm) followed by UV photon excitation at about 366 nm. VUV coherent radiation at the Lyman-a wavelength is generated by four-wave mixing of two 212.5 nm photons and one 845 nm photon in a cell filled with a 3:1 ratio Ar−Kr mixture. Photons at 212.5 nm are produced by doubling the output of a tunable dye laser (Sirah, PESC-G-24) operating at ~425 nm, pumped by the third harmonic output of a Nd:YAG laser (Spectra Physics Pro-290). A portion of the 532 nm output of the YAG is used to pump another dye laser (Continuum ND6000) operating at ~845 nm. These beams are then focused into a cell with Kr/Ar mixing gas where four-wave mixing at 121.6 nm is generated. The remainder of the 532 nm source is used to pump a third dye laser (Radiant Dye Laser-Jaguar, D90MA), operating at ~732 nm, the output from which the frequency is doubled to ~366 nm, and used to excite the H/D atoms from the $n = 2$ level to a Rydberg state with $n = 30-80$, lying just below the ionization threshold. Any charged species formed at the tagging region by initial laser excitation are extracted away from the TOF axis by a small electric field (~30 V/cm) placed across the interaction region.

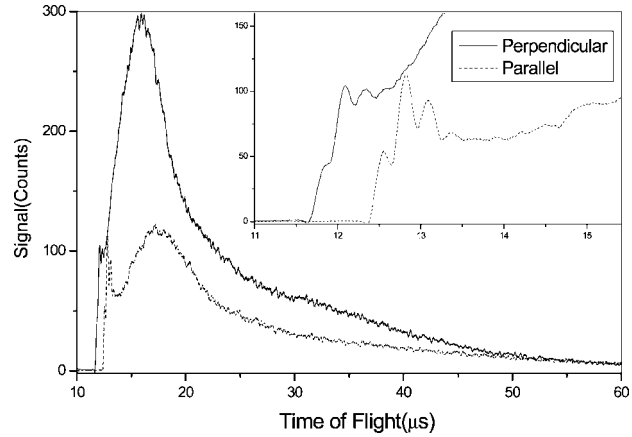

Figure 2. Time-of-flight spectra of the H atom product from the photodissociation of HN_3 at 157.6 nm with the rotating detector direction perpendicular (solid line) and parallel (dashed line) to the photolysis laser polarization.

The neutral Rydberg H/D atoms then fly a certain distance (~333 mm) to reach a MCP detector with a fine metal grid (grounded) in the front. After passing through the grid, the Rydberg tagged atoms are then immediately field-ionized by the electric field applied between the front plate of the Z-stack MCP detector and the fine metal grid. The signal detected by the MCP is then amplified by a fast preamplifier, and counted by a multichannel scaler.

HN_3 was prepared by heating sodium azide (NaN_3) in excess stearic acid under vacuum for 6−7 h at ~90−100 °C. DN_3 was produced by reacting NaN_3 with an excess of deuterated phosphoric acid, which is generated by reacting D_2O with P_2O_5 under vacuum conditions. The HN_3/DN_3 sample was stored in a stainless steel container and He gas was immediately filled to produce a mixture of 2.5% HN_3 (DN_3) in He. Purity was checked by mass spectrometry (SRS, RGA200).

3. Results and Discussions

3.1. Photodissociation of HN_3. The time-of-flight spectra (TOF) of the H-atom product from the HN_3 photodissociation at 157.6 nm were measured using the HRTOF technique described above. Two TOF spectra were obtained with the rotating detector direction parallel and perpendicular to the photolysis laser polarization. The TOF spectrum at the magic angle was also measured to check the accuracy of the polarization direction.

3.1.1. Product Translational Energy Distribution. Figure 2 shows the TOF spectra at the parallel and perpendicular directions. The perpendicular direction is the direction of the molecular beam, whereas the parallel direction is perpendicular to the molecular beam. The velocity of the parent molecular beam leads to the shift of the TOF spectra in Figure 2. The two TOF spectra have been converted to the total product translational energy distributions in the center-of-mass frame, as shown

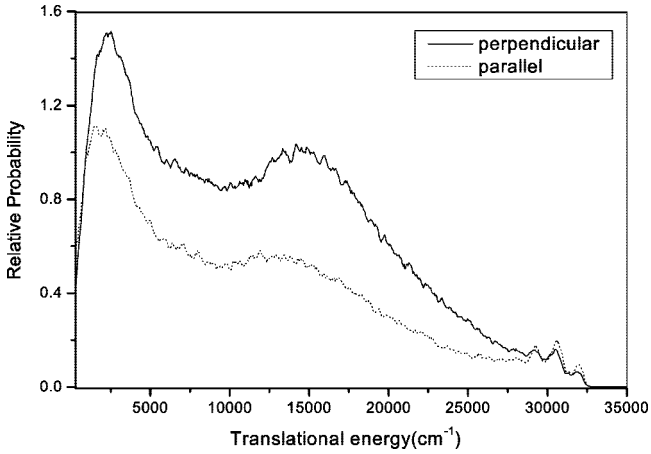

Figure 3. Product translational energy distribution derived from the experimentally measured H atom TOF spectra recorded at perpendicular and parallel direction.

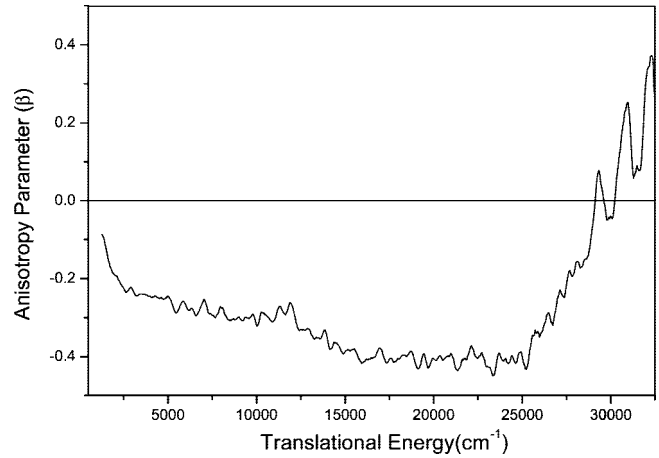

Figure 4. Anisotropy parameter β as a function of the total translational energy of HN_3 photodissociation at 157.6 nm.

in Figure 3. Obviously, the translational energy spectra are composed of three features: a slow and broad H-atom feature peaking at ~2400 cm^{-1}, a fast and broad H-atom feature peaking at ~15,000 cm^{-1} and a very fast H-atom feature with some vibrational structure near the energetic limit.

Because the momentum and energy are conserved in the photodissociation process, the product internal energy (E_{int}) deposited into the N_3 product can be determined:

$$E_{int}(N_3) = h\nu + E_{int}(HN_3) - D_0(H-N_3) - E_{trans} \quad (3)$$

where $h\nu$ is the photon energy of the photolysis laser and $E_{int}(HN_3)$ is the internal energy of the HN_3 molecule, which was set to zero because the HN_3 molecule is cooled down to very low temperature in the supersonic expansion. Using this equation, the product translation energy distribution can be converted to the N_3 product internal energy distribution.

From eq 3 if the maximum translational energy limit (E_{trans}^{max}) in the product translational energy distribution corresponds to the N_3 ground ro-vibrational state, i.e., $E_{int}(N_3) = 0$, $D_0(H-N_3)$ should be equal to $h\nu - E_{trans}^{max}$. The extrapolated onset of the maximum in Figure 3 yields $D_0(H-N_3) = 30920 \pm 100$ cm^{-1}. The error limit is due to the uncertainty in determining the threshold, the photolysis laser line width and the resolution of the TOF spectrometer. Our present result is very close to the recent experimental value obtained by Cook et al.,[14] $D_0(H-N_3) = 30970 \pm 50$ cm^{-1}, and by Zhang et al.,[16,17] $D_0(H-N_3) = 30910 \pm 100$ cm^{-1}.

From the translational energy distributions shown in Figure 3, the average translational energy, $\langle E_{trans} \rangle$ is determined to be about 35%. By comparison of this value with the recent experimental results at other photolysis wavelengths (73% at 248 nm, 64.6% at 230 nm, and 49% at 193.3 nm),[15,17] it is obvious that more available energy is deposited into the N_3 product internal energy as photolysis energy increases.

3.1.2. Product Anisotropy Distribution. The product angular distribution has also been determined in this experiment using linearly polarized 157.6 nm photolysis laser radiation. Linearly polarized light preferentially excited those HN_3 molecules with their electronic transition dipole parallel to the electric vector **E** of the polarized laser radiation. The photofragment angular distribution is given by[20]

$$I(\theta) = (1/4\pi)[1 + \beta P_2(\cos\theta)] \quad (4)$$

where β is the anisotropy parameter ($-1 \le \beta \le 2$), θ is the angle between the electric vector **E** and the recoiling velocity vector of the H-atom product (the direction of detection), and $P_2(\cos\theta)$ is the second Legendre polynomial. Figure 4 shows the translational energy dependent product anisotropy parameter obtained at 157.6 nm photolysis. Clearly, the anisotropy β parameter changes considerably from low to high translational energy. In the translational energy range of 1000−25000 cm^{-1}, the anisotropy parameter goes down from about −0.1 to −0.4 slowly and in the range 25000−32000 cm^{-1}, the product anisotropy parameter increases to about 0.2. The negative β value in the region 1000−25000 cm^{-1} indicates a perpendicular electronic transition. The dissociation dynamics in the range 25000−32000 cm^{-1} are clearly different from that in the lower energy region. In addition, there are some oscillations at high translational energy near the energetic limit. The oscillation structure in β seems to be coincident with the peaks in the translational energy distribution. Comparing with other wavelengths, where the anisotropy parameter (β) was found to be negative (−0.56 at 266 nm, −0.72 at 248 nm and ~0 at 193 nm, respectively), the anisotropy parameter at 157 nm is more complicated. The structure in the energy distribution as well as the varying β parameter suggests that the 157.6 nm photodissociation proceeds via multiple dissociation pathways.

3.1.3. Dissociation Channels. From the translational energy distribution obtained in this experiment, it appears that there are three possible channels: the slower H atom channel peaking at 2400 cm^{-1}, the fast broad channel peaking at 15000 cm^{-1}, and the fast structured channel near the energetic limit. In the translational energy range of 25000−32000 cm^{-1}, the several peaks are observed and can be assigned to the vibrational levels of the ground electronic state $N_3(\tilde{X}^2\Pi_g)$ product. The peaks in the $E_{int}(N_3)$ distribution in the range of 25000−32000 cm^{-1}, shown in Figure 3 are separated by ~1300 cm^{-1} and have widths of ~700 cm^{-1}. The two spin−orbit states, $\tilde{X}^2\Pi_{3/2}$ and $\tilde{X}^2\Pi_{1/2}$, of the N_3 product are only separated by 71.3 cm^{-1},[21] which are not resolvable in this experiment.

The electronic transition from $\tilde{X}^2\Pi$ to the low-lying excited $^2\Sigma$ state of the N_3 product was studied using LIF,[21,22] and the recommended vibrational frequencies of symmetric stretching ν_1, bending ν_2, and asymmetric stretching ν_3 are 1320, 457, and 1645 cm^{-1}, respectively. According to these vibrational frequencies, the observed vibrational structure in the translational energy distribution could be assigned to a progression involving the N_3 symmetric stretching mode ν_1. In one of the simulations, we have included only the progression of the ($\nu_1$00) vibrational series, and the simulation is not satisfactory. However, by including the series of ($\nu_1$10), the fitting to the translational

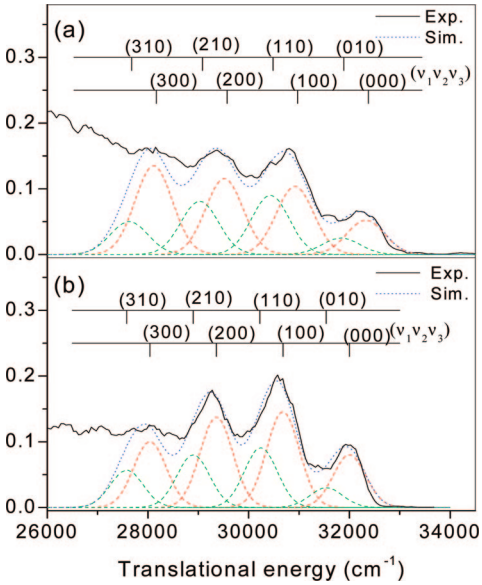

Figure 5. Experimentally derived internal energy profiles together with simulations including progressions in the ($\nu_1$00) and ($\nu_1$10) modes. The detector direction is (a) perpendicular and (b) parallel to the photolysis laser polarization.

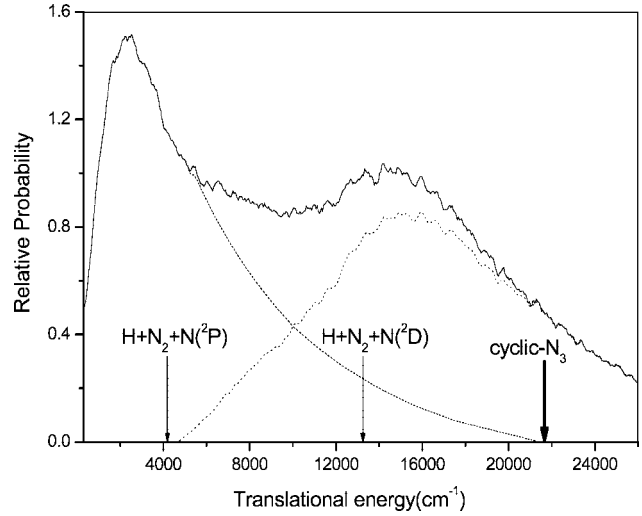

Figure 6. Broad and structureless translational energy distribution for photolysis of HN_3 at 157.6 nm. Two channels are observed: the low translational energy channel (dashed line) is consistent in energy release with formation of cyclic-N_3, the downward pointing arrows show the predicted maximum translational energy for the H + cyclic-N_3, H + N_2 + N(^{2}D), and H + N_2 + N(^{2}P), respectively; the high translational energy channel (dotted line) produces linear-N_3 products.

energy distribution in that region is much improved, as shown in Figure 5. This suggests that the N_3 products with bending excitation are also likely present. It is interesting to point out that such low vibrational states of the linear N_3 product are observed so clearly. This structure is quite similar to the dissociation structure observed at about 240 nm excitation, which is clearly due to the $\tilde{A}^1A''$ state dissociation. Therefore, it is likely that this structured feature observed in this work is due to an indirect dissociation process: a fast conversion to the $\tilde{A}^1A''$ state from the $\tilde{D}^1A'$ state and then a direct dissociation to the H + N_3(X) channel from the $\tilde{A}^1A'$ spmstate. Another interesting observation of this process is the large change of the anisotropy parameter from −0.4 to +0.2. This is very different from the $\tilde{A}$ state dissociation at about 240 nm, in which the anisotropy parameter remains almost constant. It indicates that the excited molecules in the $\tilde{D}^1A'$ state live at least for a short period of time (likely a few vibration periods). The dynamical origin of such behavior is, however, not immediately clear. This large change of the anisotropy parameter could be induced by the suggested fast conversion process between the $\tilde{D}^1A'$ state and the $\tilde{A}^1A$" state if conical intersections are involved.

In addition to the structured feature, the fast broad feature peaking at 15000 cm^{-1} is important. It also appears that its translational energy distribution goes up to the energy limit of the ground electronic state of the N_3 product, and therefore the dissociation product of this feature should be the ground state N_3. It appears that the dissociation process has an anisotropy parameter of −0.4, which is nearly independent of the translational energy, indicating that this is likely a rather direct dissociation process from the $\tilde{D}^1A'$ state to form the H + l-N_3(X) channel. And the time scale for the dissociation process likely not much longer than one rotational period of the parent molecule. This feature is very similar to that observed at 193.3 nm[15,17] and also at 199 nm,[16] in which the dissociation processes are almost from the $\tilde{B}^1A'$ and C^1A'' state to form the H + l-N_3(X) channel. It is not clear, however, whether this channel occurs directly on the $\tilde{D}^1A'$ state or converts to another lower electronic state then dissociate.

The slow product channel peaks at about 2400 cm^{-1} in the translational energy distribution and its anisotropy parameter changes from −0.1 to −0.4 as the translational energy increases. Considering the theoretical predicted energetic values of cyclic-N_3, which lies about 30 kcal/mol above the ground state of linear-N_3 with a 32 kcal/mol barrier to the linear structure,[23–25] this slow channel observed here could be the formation of cyclic-N_3 in the HN_3 photodissociation. It is necessary to point out that this slow feature is very similar to that in the 193 nm photodissociation,[17] which is also assigned to the cyclic-N_3 formation channel with a branching ratio of less than 10%. Cyclic-N_3 formation has also been reported in the 157 nm photolysis of ClN_3. Photoproduct translational energy measurements by Samartzis and Wodtke[26] revealed a single-peaked distribution for an N_3-formation channel with maximum and minimum translational energies matching the theoretically predicted minimum and maximum binding energies of cyclic-N_3, respectively. Obviously, the slow product channel peaks in the 157 nm photodissociation of HN_3 is similar to that for ClN_3. From the simulation shown in Figure 6 assuming the energetic limit for this channel is the same for the cyclic-N_3 formation, the percentage of the slow-H channel is determined to be ∼50%. This measured ratio is considerably larger than the branching ratio of the slow channel of HN_3 photolysis from 193 to 220 nm.

In addition to this cyclic-N_3 formation channel, there are also possible triple product channels that might contribute to the slow H atom channel. The energetically allowed triple product channels that generate H atoms in the photolysis of HN_3 at 157.6 nm are

$$HN_3(\tilde{X}^1A') \rightarrow H(^2S) + N_2 + N(^4S) \qquad \Delta E = 32960\ cm^{-1} \tag{5}$$

$$H(^2S) + N_2 + N(^2D) \qquad \Delta E = 13780\ cm^{-1} \tag{6}$$

$$H(^2S) + N_2 + N(^2P) \qquad \Delta E = 4180\ cm^{-1} \tag{7}$$

Among these channels, channel 5 is spin forbidden. The energetic limit of the product translational energy for channel

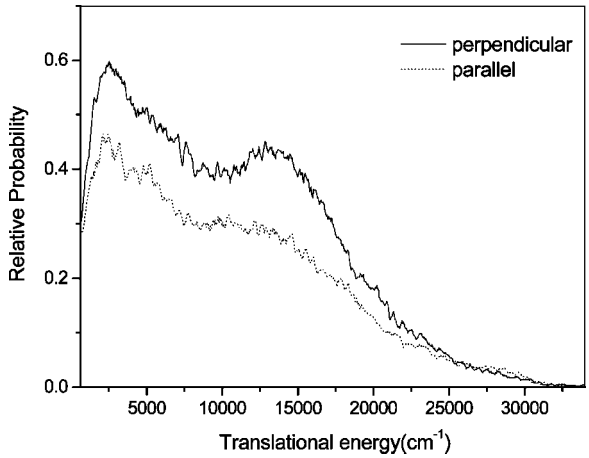

Figure 7. Product translational energy distribution derived from the experimentally measured D atom TOF spectra recorded at perpendicular and parallel direction.

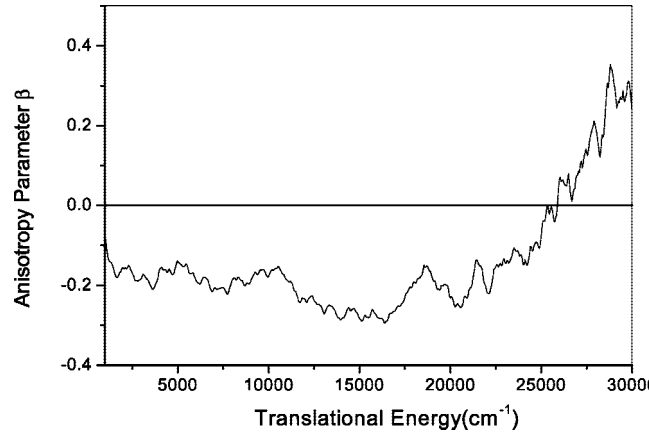

Figure 8. Anisotropy parameter β as a function of the total translational energy of DN_3 photodissociation at 157.6 nm.

6 is 13780 cm^{-1}, whereas that for channel 7 is 4180 cm^{-1} (as down pointing arrows in Figure 6). Clearly, the energetic limit for channel 7 is much too low for the slow H-atom channel which peaks at about 2400 cm^{-1} and seems to extend toward much higher energy. Therefore, contribution to the slower H-atom channel from the channel 7 should be not significant. Contribution to the slow H-atom channel from the $H(^2S) + N_2 + N(^2D)$ channel, however, cannot be ruled out because the energetic limit of the slow H-atom channel cannot be determined exactly and it seems that the energetic limit of this channel is more or less within the range of that limit. The slow H-atom channel seems to have a small changing anisotropy parameter from -0.1 to -0.4 in the lower energy region. This might be caused by the two possible channels in which the two channels have different anisotropy parameters and their translational energy distributions are different.

3.2. Photodissociation of DN_3. To understand the isotope effect on the photodissociation of HN_3, photodissociation of DN_3 at 157.6 nm has also been investigated. Time-of-flight spectra of the D-atom product from DN_3 photolysis were measured at two laboratory angles in a similar way to HN_3 photolysis except using the D-atom Rydberg tagging TOF technique. The experimental TOF spectra are then converted to the product translational energy distribution. Figure 7 shows the total product translational energy distributions of the DN_3 photodissociation at 157.6 nm. Two broad peaks are observed, similarly to that in HN_3. The vibrational structure near the energetic limit is, however, not well resolved. It appears that isotope substitution has a large effect on this channel. From the anisotropy parameter plot shown in Figure 8, the high energy section from 25000 to 32000 cm^{-1} still shows a large change from -0.2 to $+0.3$. This indicates that this fast channel might still exist but with much smaller contribution in the case of DN_3. We have suggested that this fast feature with vibrational structure might occur via coupling between the $\tilde{D}^1A'$ state and the $\tilde{A}^1A''$ state. If this is the case, the D atom substitution could affect this coupling considerably. The two broad features in the DN_3 photodissociation at 157.6 nm is, however, very much similar to that of HN_3 in terms of the translational energy distributions and the anisotropy parameter distributions. However, the branching ratio of the slower channel in the DN_3 photolysis, which is determined to be 64%, is significantly larger than that of HN_3 (50%). Because velocities of the D-atom passing through the transition state will be approximately half-that of H-atom, it is possible that more time is available for the N-atom motion that is required to close the ring for the cyclic-N_3 formation channel in the case of DN_3. This isotope effect is similar to that observed previously by Zhang et al. in the HN_3 photolysis around 200 nm.[16]

4. Conclusions

The 157.6 nm photodissociation of HN_3/DN_3 has been investigated using HRTOF technique. Time-of-flight spectra of the H/D atom product were measured at the detection direction both perpendicular and parallel to the photolysis laser polarization. Total product translational energy distributions and the product angular anisotropy parameters were also determined. Three H atom channels have been observed from the translational energy distributions. The vibrational structure in the fast H-atom channel have been assigned to the progressions of the ($\nu_1$00) and ($\nu_1$10) vibrational series. This channel likely occurs via a fast conversion from the $\tilde{D}^1A'$ state to the $\tilde{A}^1A''$ state, and then dissociates on the $\tilde{A}^1A''$ surface. The translational energy distribution of the slow H-atom channel is energetically consistent with the cyclic-N_3 formation channel and the three-body dissociation channel: $H(^2S) + N_2 + N(^2D)$. The fast broad channel peaked at 15000 cm^{-1} is clearly a linear-N_3 formation, similar to that at 193.3 nm. Photodissociation dynamics of DN_3 have also been investigated. Noticeable isotope effects on the dissociation dynamics have been detected, in which the slow H-atom products are more pronounced.

Acknowledgment. This work was supported by Chinese Academy of Sciences via the grant of the CAS international collaboration group, and also by the Ministry of Science and Technology of China and the National Natural Science Foundation of China.

References and Notes

(1) Okabe, H. *Photochemistry of Small Molecules*; Academic Press: New York, 1978.
(2) Friedmann, A.; Soliva, A. M.; Nizkorodov, S. A.; Bieske, E. J.; Maier, J. P *J. Phys. Chem.* **1994**, *98*, 8896.
(3) Okabe, H. *J. Chem. Phys.* **1968**, *49*, 2726–2733.
(4) Orlando, J. J.; Tyndall, G. S.; Betterton, G. A.; Lowry, J.; Stegall, S. T. *Environ. Sci. Technol.* **2005**, *39*, 1632.
(5) Chu, J. J.; Marcus, P.; Dagdigian, P. J. *J. Chem. Phys.* **1990**, *93*, 257.
(6) Rohrer, F.; Stuhl, F. *J. Chem. Phys.* **1988**, *88*, 4788.
(7) Gericke, K. H.; Lock, M.; Fasold, R.; Comes, F. J. *J. Chem. Phys.* **1992**, *96*, 422.
(8) Gericke, K. H.; Hass, T.; Lock, M.; Thienl, R.; Comes, F. J. *J. Phys. Chem.* **1991**, *95*, 6104.
(9) Hawley, M.; Baronavski, A. P.; Nelson, H. H. *J. Chem. Phys.* **1993**, *99*, 2638.

(10) Gericke, K. H.; Lock, M.; Comes, F. J. *Chem. Phys. Lett.* **1991**, *186*, 427.
(11) Lock, M.; Gericke, K. H.; Comes, F. *J. Chem. Phys.* **1996**, *213*, 385.
(12) Haas, T.; Gericke, K. H.; Maul, C.; Comes, F. J. *Chem. Phys. Lett.* **1993**, *202*, 108.
(13) Cook, P. A.; Langford, S. R.; Ashfold, M. N. R. *Phys. Chem. Chem. Phys.* **1999**, *1*, 45.
(14) Cook, P. A.; Jimeno, P.; Ashfold, M. N. R.; Balint-Kurti, G. G.; Dixon, R. N. *Phys. Chem. Chem. Phys.* **2002**, *4*, 1513.
(15) Zhang, J. S.; Xu, K. S.; Amaral, G. *Chem. Phys. Lett.* **1999**, *299*, 285.
(16) Zhang, J.; Zhang, P.; Cheng, Y.; Yuan, K.; Harich, S. A.; Wang, X.; Wang, Z.; Yang, X.; Morokuma, K.; Wodtke, A. M. *Phys.Chem. Chem. Phys.* **2006**, *8*, 1690.
(17) Zhang, J.; Yuan, K.; Cheng, Y.; Harich, S. A.; Wang, X.; Yang, X.; Wodtke, A. M. *Chin. J. Chem. Phys.* **2007**, *20*, 345.
(18) Schneider, L.; Meier, W.; Welge, K. H.; Ashfold, M. N. R.; Western, C. *J. Chem. Phys.* **1990**, *92*, 7027.
(19) Schnieder, L.; Seekamp-Rahn, K.; Wrede, E.; Welge, K. H. *J. Chem. Phys.* **1997**, *107*, 6175.
(20) Zare, R. N. *Mol. Photochem.* **1972**, *4*, 1.
(21) Douglas, A. E.; Jones, W. J. *Can. J. Phys.* **1965**, *43*, 2216.
(22) Beaman, R. A.; Nelson, T.; Richards, D. S.; Setser, D. W. *J. Phys. Chem.* **1987**, *91*, 6090.
(23) Babikov, D.; Zhang, P.; Morokuma, K. *J. Chem. Phys.* **2004**, *121*, 6743.
(24) Zhang, P.; Morokuma, K.; Wodtke, A. M. *J. Chem. Phys.* **2005**, *122*, 014106.
(25) Continetti, R. E.; Cyr, D. R.; Osborn, D. L.; Leahy, D. J.; Neumark, D. M. *J. Chem. Phys.* **1993**, *99*, 2616.
(26) Samartizis, P. C.; Lin, J. J.; Ching, T. T.; Chaudhuri, C.; Lee, S. H.; Wodtke, A. M. *J. Chem. Phys.* **2007**, *126*, 041101.

JP800062T